Wake interaction and power production of variable height model wind farms

Vested, Malene Hovgaard; Hamilton, N.; Sørensen, Jens Nørkær; Cal, R. B.

Published in:
Journal of Physics: Conference Series (Online)

Link to article, DOI:
10.1088/1742-6596/524/1/012169

Publication date:
2014

Document Version
Publisher's PDF, also known as Version of record

Wake interaction and power production of variable height model wind farms

2014 J. Phys.: Conf. Ser. 524 012169

(http://iopscience.iop.org/1742-6596/524/1/012169)

Wake interaction and power production of variable height model wind farms

M. H. Vested,[1] N. Hamilton,[2] J. N. Sørensen[1] & R. B. Cal[2]

[1]Department of Wind Energy, Technical University of Denmark, Lyngby, Denmark
[2]Department of Mechanical and Materials Engineering, Portland State University, Portland, OR, USA

E-mail: cal@me.pdx.edu

Abstract. Understanding wake dynamics is an ongoing research topic in wind energy, since wakes have considerable effects on the power production when wind turbines are placed in a wind farm. Wind tunnel experiments have been conducted to study the wake to wake interaction in a model wind farm in tandem with measurements of the extracted power. The aim is to investigate how alternating mast height influences the interaction of the wakes and the power production. Via the use of stereo-particle image velocimetry, the flow field was obtained in the first and last rows of the wind turbine array as a basis of comparison. It was found that downstream of the exit row wind turbine, the power was increased by 25% in the case of a staggered height configuration. This is partly due to the fact that the taller turbines reach into a flow area with a softened velocity gradient. Another aspect is that the wake downstream of a tall wind turbine to some extent passes above the standard height wind turbine. Overall the experiments show that the velocity field downstream of the exit row changes considerably when the mast height is alternating.

1. Introduction

In recent years, the development in wind farm installations has seen two major trends. The wind farms increase in size by the addition of turbines and the size of the wind turbines increase in the diameter of the rotor and subsequently the height of the mast. The latter, taller masts, can lend itself to entrain more energy from the above flow, since they operate at higher altitudes where the turbine is less affected by the effects. However, when wind turbines are deployed in wind farms, the power output tends to decrease due to wake to wake interactions. Therefore, further understanding these interactions in large wind farms is crucially important in the quest to optimize power extraction. The development in wind farm installations therefore poses two questions; the one being how to arrange the wind turbines in the wind farm to optimize the power output, the other being how the wakes develop downstream of the wind turbines.

When considering an array, the flow complexity is naturally increased and several studies have elucidated flow physics within this setting. Flow characteristics within the array of model wind farm were performed by Chamorro and Porté-Agel to understand the effects of surface roughness on the array. It was found that the velocity fluctuations are enhanced by this effect close to the wall and that the levels of turbulence are even more pronounced at the top half of the rotor. [1] The wind farm dependence on the downstream distance was documented in [2] where it was found that the flow achieves a fully developed state by the third turbine. Further studies

on placement have been carried out by observing the wake-to-wake interaction in a staggered arrangement. [3], [4] Similar results were observed in terms of an increase in power production due to the staggering as well as detailing the reduced interactions between the wakes. In the latter, a torque sensing system was employed to measure the power and the output of the wind farm was compared for two different configurations; a standard Cartesian array configuration and a row-offset configuration. It was found that the power output was increased threefold for the row-offset configuration compared to the standard configuration.

The near-wake region of a model wind turbine has been studied by Zhang *et al.* [5] using Particle Image Velocimetry (PIV). The study showed that vortices are created by the tip of the rotor blades and that the near-wake region is characterized by high three-dimensionality, turbulence heterogeneity and flow rotation. In a study by Cal *et al.* [6] measurements around a model wind farm in a wind tunnel were carried out using particle image velocimetry (PIV). It was found that the vertical fluxes of kinetic energy associated with the Reynolds shear stresses are of the same order of magnitude as the power extracted by the wind turbines. [6] It is suggested that when wind turbines are employed in arrays, the main source of energy comes from above the wind turbine canopy. These results emphasize the importance of understanding the vertical transport of energy in the wind turbine arrays in order to optimize the power generation. These processes were confirmed numerically using a drag disk model in a fully developed wind turbine array boundary layer by Calaf *et al.* [7] A similar approach has been also used by Dabiri for a wind farm composed of vertical axis wind turbines [8] and Lignarolo *et al.* on the wake of a single turbine under uniform conditions [9].

2. Theory

Following the Reynolds decomposition, u_i is decomposed into mean velocity and fluctuating velocity, respectively, $u_i = U_i + u_i'$ and the Reynolds averaged equations (RANS) follows as

$$U_j \frac{\partial U_i}{\partial x_j} = -\frac{1}{\rho}\frac{\partial P}{\partial x_i} - \frac{\partial \overline{u_i' u_j'}}{\partial x_j} - \overline{f_x}, \tag{1}$$

in which subscript i represents the index concerning the component in a particular direction. The force term $\overline{f_x}$ represents the force introduced to the flow by the disturbance of the wind turbines. Since this force mainly acts in the streamwise direction it has been subscripted with an x. The viscous and unsteady terms are neglected as shown in [6].

Multiplying equation 1 by the mean velocity U_i results in the equation for the mean kinetic energy which is defined as $K = \frac{1}{2}U_i^2 = \frac{1}{2}(U^2 + V^2 + W^2)$. When the wind farm can be approximated to be very large and considering the streamwise direction, the developing terms on the left-hand side and the pressure gradient in x can be neglected and the equation reduces to

$$-\overline{u'v'}\frac{\partial U}{\partial y} - \frac{\partial}{\partial y}\left(\overline{u'v'}U\right) - F(y) \approx 0, \tag{2}$$

where the production of turbulence kinetic energy is $-\overline{u_i' u_j'}\frac{\partial U_i}{\partial x_j}$, the flux of turbulence kinetic energy is $-\overline{u_i u_j'}U_i$ and the power extracted by the wind turbineis the last term. The available power $P(y)$ can thus be computed through the production of turbulence kinetic energy and the derivative of the flux of turbulence kinetic energy. These terms will therefore be of particular interest in the following analysis. Both the flux and the production depend dominantly on the Reynolds shear stress $-\overline{u'v'}$, which therefore will be considered specifically in the following analysis.

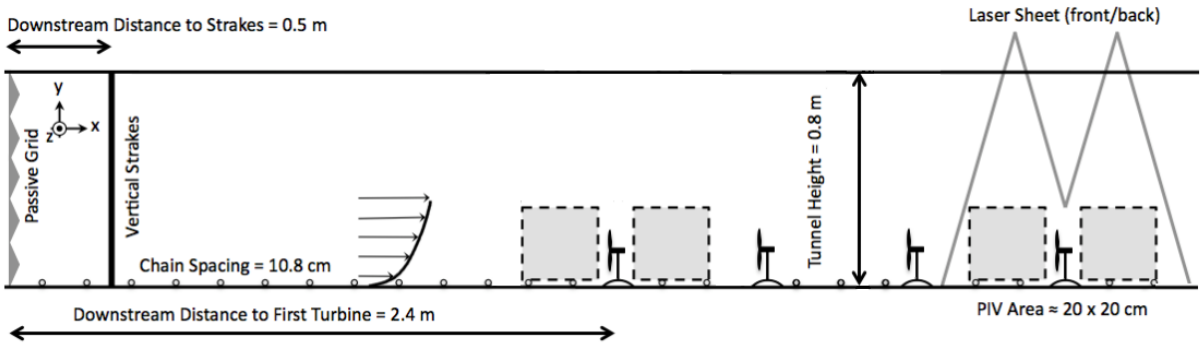

Figure 1: Schematic of the experimental setup, dimensions are not to scale. The test section is viewed from the user-side of the wind tunnel.

3. Experimental design

The experiments have been carried out at the wind tunnel facility at Portland State University. This is a return-type wind tunnel with working speeds between 3-30 m/s and a contraction ratio of 9:1. The test section is 5 m long, 0.8 m high and 1.2 m wide. In order to model the inflow, several components have been installed inside the tunnel. These conditions are depicted in fig. 1. At the entrance of the test section, a passive grid introduces turbulence to the inflow. In addition, the shape of the strakes is designed so that the flow develops a sheared inflow velocity profile. Across the floor of the test section, small-diameter chains introduce an appropriate surface roughness. Further information on the inflow characteristics and experimental conditions are presented in [4] as well as the scaling characteristics and representative Reynolds numbers. The latter discussion is further enhanced in [6], [10] and [3].

A set of 12 model turbines were fabricated in-house for the experiments. The nacelle of each wind turbine consist of an electric motor acting as a generator, which is mounted to a 1 cm hollow shaft. The motors are of the model Faulhaber GMBH & Co Series 1331T012SR with a 12 V nominal voltage and a 0.0105 A current at no load. The outside diameter of the generator is 1.3 cm. The generators were aligned with the flow with the motor shaft pointed upstream. Three blades form the rotors and each rotor blade is $6cm$ long; thus a diameter, D, of 12 cm. The rotor blades were cut out with laser from a 0.5 mm thick steel sheet and formed to shape with a pitch of 15° at the widest part of the rotor blade and a 10° pitch twist at the tip of the rotor blade. The wind turbine masts are made at two different heights, a standard mast measuring $12cm$, D, and a tall mast measuring 18.2 cm, $1.5D$. A torque sensing system was implemented in the experiment in order to measure the generated power by the wind turbines. For detailed descriptions of the torque sensing system, see [4]. The tip speeds were monitored through a Monarch optical tracker with a working range of 1-250000 rpm. Each row of model wind turbines was set to operate under loading conditions which corresponded to the peaks of their respective power curve. The rotational speed of the rotors was controlled by applying resistive electrical loads to the motor.

3.1. The wind farm configurations

Five wind turbine configurations were tested in the experiments. The objective is to make use of varying mast heights to understand the wake to wake interaction as well as its impact on the power production. In all test cases, the wind turbines were positioned in 4 rows with 3 wind turbines in each row. The spacing was kept constant at 6 rotor diameters in streamwise direction and 3 rotor diameters perpendicular to the streamwise direction. Five wind farm configurations have been investigated in which the height of the wind turbines was varied with the tall turbines

1.5 times taller than the standard. As a base case, a configuration consisting of 12 standard height wind turbines is included. The configurations are named as case A, B, C, D and E, in which A is the base case. These configurations are depicted in figures 2 and 3 in which **S** denotes standard masts equaling $1D$ in height and **T** denotes taller masts with a vertical height of $1.5D$. The staggered height configurations B and C have a tall wind turbine at the center of the front row, followed by a standard-tall-standard configuration at the center row. The flanks are the same height in B and checkered in C, see fig. 3a and 3b. The cases D and E have a standard height wind turbine at the center of the front line, followed by tall-standard-tall turbines at the center row. Case D has same height turbines at the flanks while E is a checkered configuration, see fig. 3c and 3d. In fig. 4, a side view of case D is observed. Case C and E are 'checkered-board' configurations which means that no turbine standing next to each other has same height. The C case has a tall wind turbine at the center of the front row, while the E case has a short turbine at the center of the front row, shown in fig. 3d and fig. 3b. These set-ups are included to investigate the influence of the neighboring turbines.

$\vdash S$	$\vdash S$	$\vdash S$	$\vdash S$
$\vdash S$	$\vdash S$	$\vdash S$	$\vdash S$
$\vdash S$	$\vdash S$	$\vdash S$	$\vdash S$

Figure 2: Base case configuration with standard turbines (Case A)

$\vdash T$	$\vdash S$	$\vdash T$	$\vdash S$
$\vdash T$	$\vdash S$	$\vdash T$	$\vdash S$
$\vdash T$	$\vdash S$	$\vdash T$	$\vdash S$

(a) Case B

$\vdash S$	$\vdash T$	$\vdash S$	$\vdash T$
$\vdash T$	$\vdash S$	$\vdash T$	$\vdash S$
$\vdash S$	$\vdash T$	$\vdash S$	$\vdash T$

(b) Case C

$\vdash S$	$\vdash T$	$\vdash S$	$\vdash T$
$\vdash S$	$\vdash T$	$\vdash S$	$\vdash T$
$\vdash S$	$\vdash T$	$\vdash S$	$\vdash T$

(c) Case D

$\vdash T$	$\vdash S$	$\vdash T$	$\vdash S$
$\vdash S$	$\vdash T$	$\vdash S$	$\vdash T$
$\vdash T$	$\vdash S$	$\vdash T$	$\vdash S$

(d) Case E

Figure 3: Experimental cases for varying mast height depicting row by row variations (cases B and D) and checkered board variations (cases C and E)

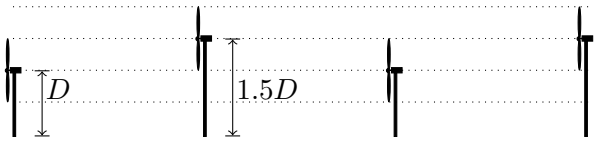

Figure 4: Wind farm configuration case D seen in profile. The standard mast wind turbines have a hub height of the same size as the rotor diameter $D = 0.12m$, while the tall mast wind turbines have a hub height of $1.52D = 0.182m$.

3.2. PIV measurements

In order to measure the flow field, stereographic Particle Image Velocimetry (SPIV) technique was employed. The seeding particles were neutrally buoyant fluid particles made of diethylhexyl sebacate. The flow was seeded by the use of Laskin nozzles prior to the flow conditioning section of the tunnel to ensure a well mixed distribution of particles in the cross-section. In each measurement window, a single laser sheet with a thickness of 1 mm was used. The laser sheet was blocked at the center to reduce reflections from the turbine. Each laser sheet had a divergence angle of less than 5 $mrad$ across the span of the measurement locations.

The SPIV data collection was carried out using a LaVision system with a Nd:Yag (532 nm, 1200 mJ, 4 ns duration) double-pulsed laser and four CCD cameras. The cameras were arranged in pairs to collect data simultaneously in two windows. The measurement windows are upstream and downstream of the centerline entrance and exit turbines. The time delay between the exposures of the camera was 130 μs and the cameras collected 2000 SPIV images at each of the four measurement planes. Before the measurements a calibration of the camera focii was carried out using a calibration plate. The calibration plate is designed with two-leveled thickness, which determines the depth of the measurement plane. The interrogation area covers approximately 0.23 m × 0.23 m with an approximate resolution of 1.5 mm.

The raw images were processed into vector fields using a multi-pass FFT based correlation algorithm of reducing size interrogation windows with a 50% overlap. The algorithm used interrogation windows twice with 64 × 64 pixels and once with 32 × 32 pixels. Successively, the vector fields were filtered to identify measurements outside of the reliable range.

4. Results

4.1. Mean velocity

The measured vector fields at the exit row in the five different wind farm configurations are analyzed here. The mean streamwise and vertical velocity are displayed in fig. 5a and fig. 5b, respectively. The contours shown depict planes in the front and aft of the last row center turbine. The mean streamwise velocity at the exit row is shown in fig. 5a. Upstream of the wind turbines, the recovery of the wake is considerably stronger in the cases where the preceding wind turbine is short, case D and E, when compared to the cases where the preceding wind turbine is tall, case B and C. The tall turbine cases observe increased velocity magnitudes below the bottom rotor tip. As expected, the effects of the wall influence the flow below the bottom tip for the case with the standard masts. Nevertheless, the shape of the wakes tend to be similar amongst the different cases at least in the rotor swept area region. Comparing the staggered height configurations to the base case, the fluid moves 6% faster in case D-E at $x/D = 2$ and 3% slower in case B-C.

In fig. 5b, the mean vertical velocity is displayed. Vertical velocities upstream of the turbine are dissimilar for the base case when compared to either cases B and C or cases D and E. A more homogeneous flow over then entire interrogation region is observed for cases D and E in which a standard height turbine on the prior row is present. The magnitude for these is roughly 0.15 m/s with the exception of close to the turbine which show a lower magnitude due to the influence of the mast and rotor. Opposite to this behavior, in cases B and C, the influence of the wall produces a relatively stronger magnitude of velocity above the nacelle. The wake area in the standard mast cases B-C has a downward motion 50% greater than in the base case at $x/D = 1.5$. These negative velocities persist over a larger downstream distance. The opposite occurs for the tall mast cases D-E where now the velocities are close to zero or are directed slightly upwards. Below hub height at $x/D = 2$, magnitudes of V are approximately 20% slower in the standard mast cases B-C compared to the base case. This effect is further intensified up to magnitudes between 60% and 70% for cases D and E, where tall turbines are present. There is an effect due to the checkered configuration in the tall exit row (case E), where below hub

height the advection of the fluid is slower than in case D, especially at $1 < x/D < 2$.

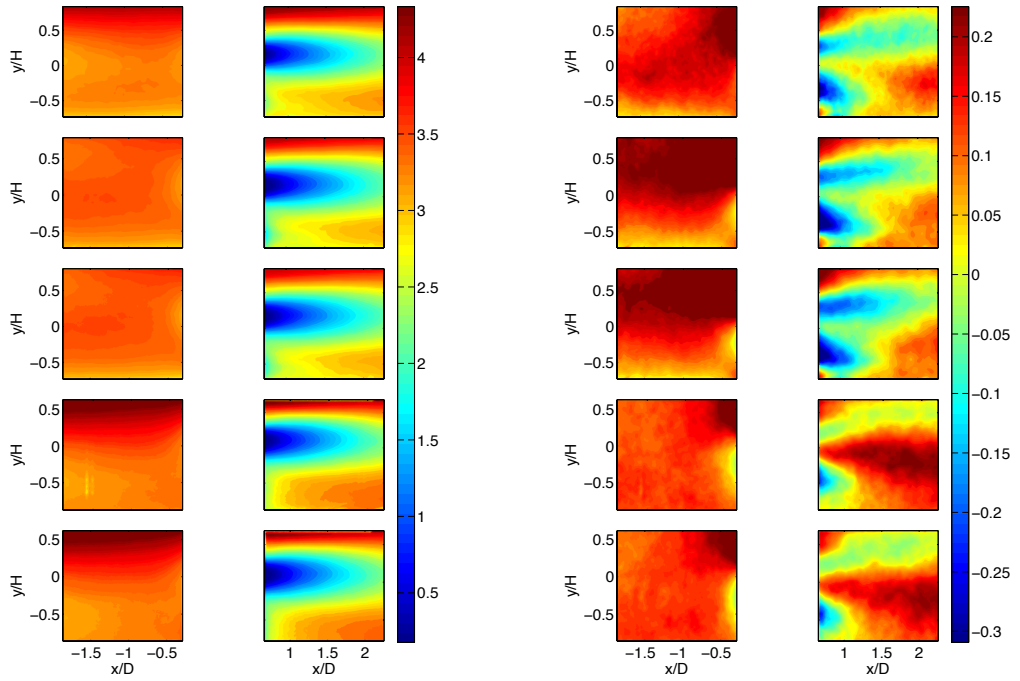

(a) Mean streamwise velocity at the exit row (b) Mean vertical velocity at the exit row

Figure 5: Mean streamwise and vertical velocity at the exit row. Cases from top to bottom are denoted as A through E, respectively. In the subsequent contours, the cases are ordered in the same fashion.

In fig. 6, vertical profiles for the mean streamwise velocity are shown and are normalized by the hub height velocity. Since the contour plots for the staggered height cases are so similar within statistical error, the checkered cases C and E overlap the cases B and D, respectively especially upstream of the turbines and in the downstream positions $x/D = 1.5$ and $x/D = 2.0$. The inflow profiles are very similar for the considered cases, especially close to the turbine where the profiles overlap below hub height. In magnitude, the maximum velocity deficit is the same in the three cases, and continue to be the same as the fluid moves downstream. Above the hub height, the fluid is transported faster in the tall mast noted by cases D & E and slower in the standard mast cases B-C compared to the base case. The same trends are seen below the bottom tip of the rotor.

4.2. Reynolds stress and flux of kinetic energy

The contours of the in-plane Reynolds shear stress $-\langle u'v' \rangle$ are shown in fig.7a. Upstream of the turbine, the base case shows behavior previously seen in [6] as there is an influence due to the top tip and bottom tip created from the previous tip and well align with the subsequent rotor. It is also evident that the stress at the top tip is greater in magnitude to that observed at the bottom tip. In cases B and C, a tall turbine is present in the previous row therefore, the stresses generated due to the bottom tip are now positioned at the height of the hub for the last turbine. The stresses although of the same order of magnitude, they persist for a longer distance. For this case, the top tip effect from the preceding turbine is not captured due to the location of the measurement window. Perhaps more interestingly, the cases D and E which possess a

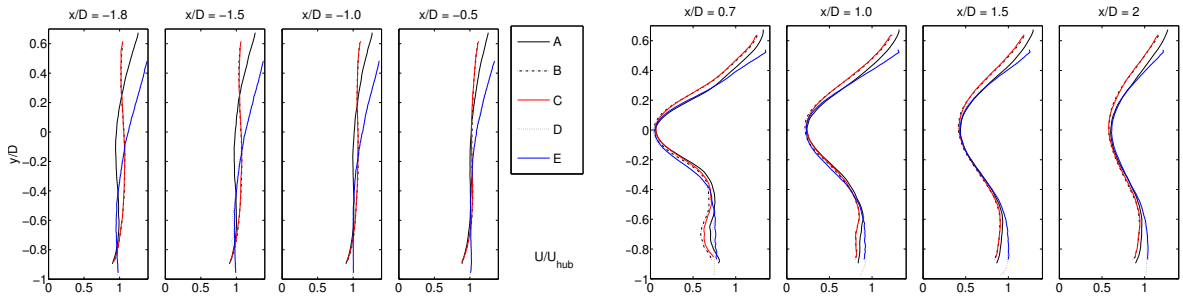

Figure 6: Vertical profile of mean streamwise velocity at exit row. The velocity is normalised with the velocity at the hub height of the standard mast turbine. The coordinate system is centered in the hub height of the respective wind turbine.

standard height turbine from the previous row tend to show magnitudes three times lower than the base case, thus pointing towards the fact that there is indeed a cumulative effect and this is attenuated due to the staggering of heights in the masts of the turbines. When considering the wake, the top and bottom tip effects are clear in each of the cases, showing positive values at the top tip and conversely negative values of $-\langle u'v' \rangle$ at the bottom tip. Furthermore, there is a decrease in magnitude at these locations when the previous turbine is tall pointing to the fact that first the turbine is located closer to the wall and second that a clear non-aligned shear stress from the previous turbine is observed as shown in cases B and C. It is important to note that the magnitude of this incoming feature is rather small with a value of approximately -0.025. Quantitatively speaking, the decreased in case B consists of 6% and 15% in case C below hub height when compared with the base case. Above the hub height these differences are amplified thus achieving values of 20% lower than the base case.

A rather drastic change is noticed when considering the tall turbines as shown in cases D and E. The values here are augmented at the bottom and top tips thus generating rather intense features. Here, it is important to note that the incoming in-plane Reynolds stress is much larger than previously observed (from cases B and C) where the turbine at the third row has a standard height. The values of the incoming Reynolds shear stress is on the order of $0.12 - 0.17$. This is an important factor as it leads to the conclusion that the incoming turbulence promotes a larger Reynolds shear stress at the particular turbine. Furthermore, the alignment of these Reynolds shear stress features must not exactly correspond to the top and bottom tips but rather be slightly offset as observed here. The percent in increase for these features once again varies in position (above or below hub height) when compared to the base case. The proliferation of the value consists of a 25% increase above the hub height and below the hub height is dependent on whether the case is checkered or not (case E and D, respectively) where the intensification is found to be 35 and 15%.

One of the most important quantities in the sense of power production is the flux of kinetic energy. It has been shown in [6] that the vertical flux is the main mechanism in entraining energy from the flow in a large wind farm. In the following, the main contributor to the flux, $-\langle u'v' \rangle U$, is considered as shown in the fig. 7b. It is clear that the features for each of the cases resemble those as discussed in fig. 7a. When considering the increase or decrease of flux as a function of a particular case when compared to the base line, it is seen that the flux has decreased approximately 22% above the hub height (cases B and C) and increased 45% for cases (D and E). Below the hub height, the decrease for cases B and C is comprised of 12% and 17%, respectively; while for cases D and E, possessing a taller mast, the flux is increased by 10% in case D and as much as 34% in case E. As a result, case E contains larger magnitudes (positive or negative) than the other configurations. It is clear then that not only increasing the mast height

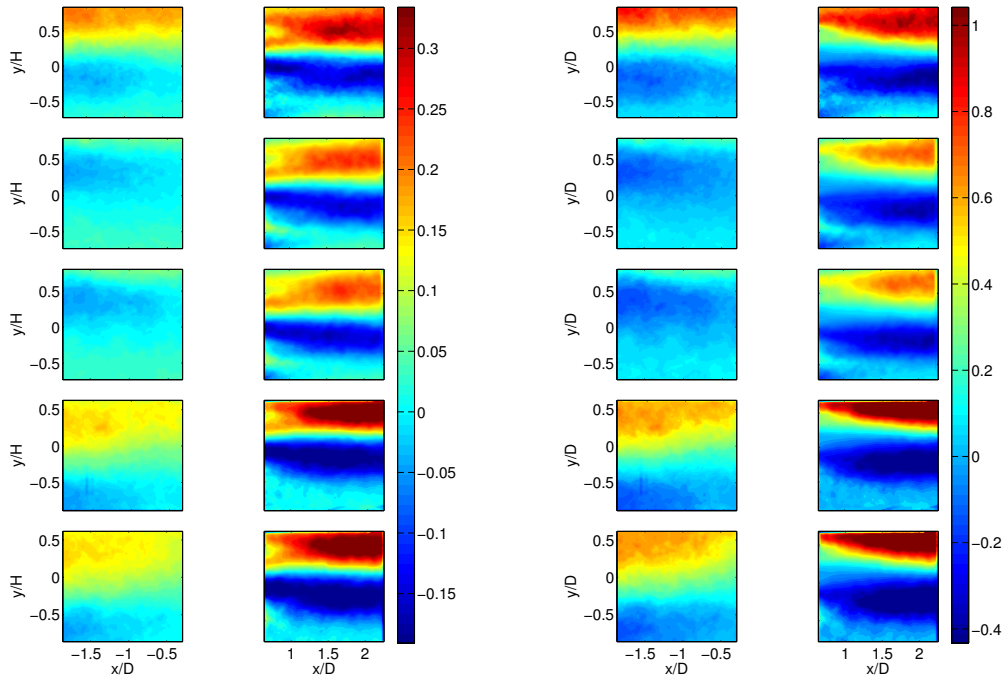

(a) In-plane Reynolds shear stress $-\langle u'v' \rangle$ (b) Flux of turbulence kinetic energy $-\langle u'v' \rangle U$

Figure 7: In-plane Reynolds stress and flux of turbulence kinetic energy at the exit row.

affects this quantity but also alternating the heights (checkered board) suggests an influence in the flux. This, consequently, points to the idea that turbines which are not directly in front of the turbine of interest also leave an imprint on the given features for that turbine.

Vertical profiles of the flux of turbulence kinetic energy are shown in fig. 8 to observe the streamwise development of the quantity for those presented in the contour plot as shown in figure 7b. First analyzing the inflow profiles, the flux is close to zero for all cases at the bottom tip position. Immediately after, these values become positive above the bottom tip for the tall mast cases D and E. For the standard mast cases B and C, the values become positive above the top tip. The 'intermediate' values occur for the base case (case A), where the flux becomes positive right the hub height. Past the turbine in the outflow, the profiles follow closely in the two first distance $x/D = 0.7$ and $x/D = 1.0$ except above the top tip of the rotors. The standard mast cases show smaller fluxes above hub height but follow the base case closely below. The tall mast cases D-E have larger extrema than the base case. At the downstream distance $x/D = 2$, the case D has larger positive flux at the top tip while the checkered case E has larger negative fluxes below hub height.

4.3. Power

In fig. 9a, the measured power for at standard mast and a tall mast single wind turbine is plotted against the tip speed of the rotor blades ω. The power measurements show a clear increase in power output for a single wind turbine when the mast height is increased. For the standard mast turbine, the measured power has a maximum of $0.14W$ while for the tall mast turbine the maximum is $0.20W$. Consequently, the tall mast turbine produces 43% more than the standard mast turbine when standing alone. The measured power produced by the center turbine in the exit row is shown in fig. 9b for case A, B, D and E. It is observed that the center turbine in the base case A produces $0.08W$ while the corresponding turbines in the staggered height cases B, D

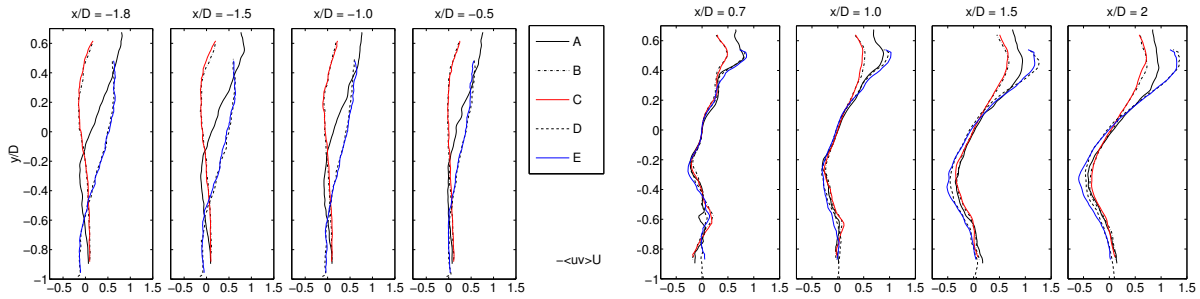

Figure 8: Vertical profile of the kinetic energy flux at the exit row. The coordinate system is centered at the hub height of the respective wind turbine.

and E produce between $0.1W$ and $0.11W$. Comparing the front row and the exit row in the base case, the production is decreased by 43% at the exit row. For the staggered height configuration B, which has standard mast turbines at the exit row, the production at this wind turbine is only 29% less than at the front row. The overall conclusion is that there is an immediate power gain for a standard wind turbine at the fourth row. Comparing the tall mast turbine at the front row to a tall mast turbine at the exit row, the power is decreased by between 50% in case D and 45% in case E. Interestingly, the difference in power production between a tall mast and a standard mast seems to diminish at the exit row in the staggered height configurations. It is seen that case B (standard mast) produces the same power as case D (tall mast). The measured power for each wind turbine in the configurations A, B, D and E has been tabulated in table 1 in Watt. It is seen that the total power output is increased by 20-40% in the variable height configurations.

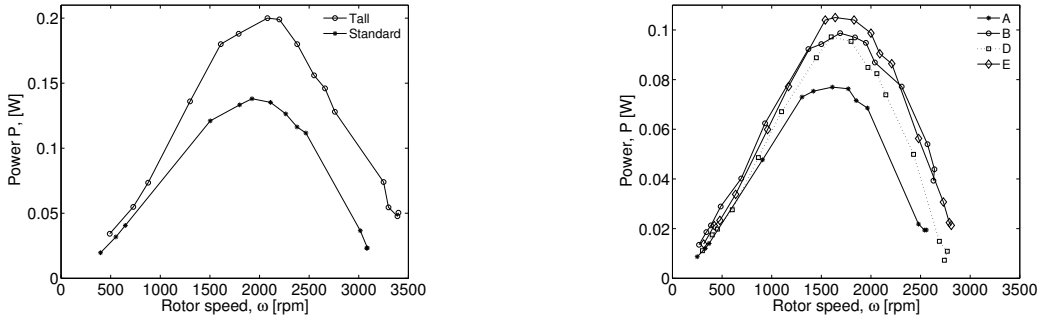

(a) Measured power at the center wind turbine at the front row

(b) Measured power in the center wind turbine at the exit row

Figure 9: Power production, P *versus* rotor speed, ω

5. Conclusions

Experimental investigations on a model wind farm have been made using stereographic PIV for varying height of wind turbine masts. In obtaining high spatially resolved instantaneous velocity fields, mean and fluctuating quantities are analyzed for the various experimental cases. The mean streamwise and vertical velocities as well as the in-plane Reynolds stress and mean kinetic energy flux are presented. Additionally, a torque sensing system was mounted on the center row turbine in the front and exit rows, allowing for a direct measurement of the power.

Table 1: Power for each turbine based on the particular case.

Configuration	Row 1	Row 2	Row 3	Row 4	Total
A $(S-S-S-S)$	0.14	0.08	0.08	0.08	0.38
B $(T-S-T-S)$	0.20	0.11	0.10	0.10	0.51
D $(S-T-S-T)$	0.14	0.14	0.10	0.10	0.48
E $(S-T-S-T)$	0.14	0.12	0.09	0.11	0.46

Five different configurations of the wind farm were considered and PIV results around the center turbine at the exit row were presented. It was found that the wake effects change remarkably in a wind farm configuration with alternating mast height. The mean streamwise velocity depicts clear effects due to the wall as seen for the standard masts, which are otherwise considered negligible for the near wake in the taller masts. The mean vertical velocity is more influenced, where the features tend to be lessened in magnitude for the standard masts in the varying height case. In the presence of taller masts, these effects are very well enhanced.

The in-plane Reynolds shear stress was analyzed and similar behavior was also observed by the kinetic energy flux which produced the following conclusions. The flux of turbulence kinetic energy at the top tip was decreased by 22% in the standard mast cases compared to the base case, and increased by 45% in the tall mast cases. In addition, at the bottom tip the flux decreased in the standard mast cases and increased in the tall mast cases. It is also observed that the checkered configurations amplified this effect at the bottom tip, especially in the tall mast case E. In other words, it was found that the effects of a checkered mast configuration were stronger at the tall masts than at the standard masts.

The power was measured at the exit row in the staggered height configurations and compared to the base case of all same-height wind turbines. It was found that the power produced by a standard height wind turbine increased by 25% in compared to the base configuration. Interestingly, the difference in power production between a tall mast and a standard mast seems to diminish at the exit row in the staggered height configurations. It is seen that case B (standard mast) produces the same power as case D (tall mast). This might prove a powerful result in energy optimization of future wind farms.

Acknowledgments

This work was in part funded by the U.S. National Science Foundation under grant *ECCS-1032647*.

References

[1] Chamorro L P and Porté-Agel F 2009 *Boundary-Layer Meteorology* **132** 129–149
[2] Chamorro L P and Porté-Agel F 2011 *Energies* **4** 1916–1936
[3] Chamorro L, Arndt R and Sotiropoulos F 2012 *Wind Energy* **15** 733–742
[4] Hamilton N, Melius M and Cal R B 2014 *Wind Energy* n/a–n/a ISSN 1099-1824
[5] Zhang W, Markfort C D and Porté-Agel F 2012 *Experiments in Fluids* **52** 1219–1235
[6] Cal R B, Lebron J, Castillo L, Kang H S and Meneveau C 2010 *Journal of Renewable and Sustainable Energy* **2** 1–25
[7] Calaf M, Meneveau C and Meyers J 2010 *Physics of Fluids* **22** 015110
[8] Dabiri J O 2011 *Journal of Renewable and Sustainable Energy* **3** 043104
[9] Lignarolo L E, Ragni D, Ferreira C S and van Bussel G G 2014 *Proc. 32nd ASME Wind Energy Symposium* (*AIAA Sci Tech* vol AIAA) (American Institute of Aeronautics and Astronautics)
[10] Melius M S, Tutkun M and Cal R B 2014 *Journal of Renewable and Sustainable Energy* **6** 023121